Journal of
Materials Chemistry A

Accepted Manuscript

This article can be cited before page numbers have been issued, to do this please use: C. Chang, C. Wang, R. Raja, L. Wang, C. Tsao and W. Su, *J. Mater. Chem. A*, 2018, DOI: 10.1039/C7TA07939G.

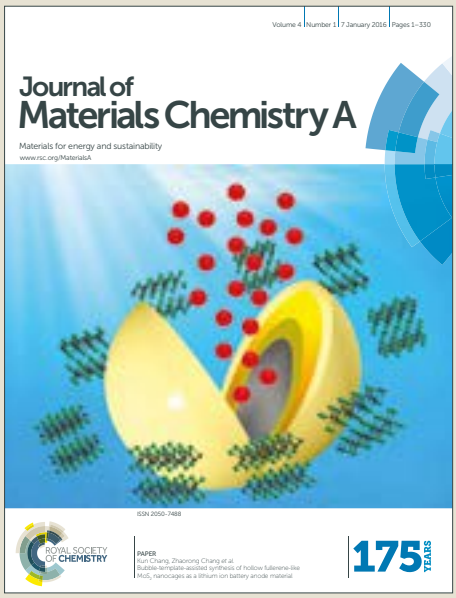

ROYAL SOCIETY OF CHEMISTRY

rsc.li/materials-a

View Article Online
DOI: 10.1039/C7TA07939G

Journal Name

ARTICLE

High efficiency bulk heterojunction perovskite solar cell fabricated from one-step solution process using single solvent: synthesis and characterization of material and film formation mechanism

Received 00th January 20xx,
Accepted 00th January 20xx

DOI: 10.1039/x0xx00000x

www.rsc.org/

Chun-Yu Chang[a†], Chieh-Ping Wang[a†], Rathinam Raja[b], Leeyih Wang[b], Cheng-Si Tsao[a,c], and Wei-Fang Su[a*]

Bulk heterojunction (BHJ) perovskite solar cells recently attract increased interest because of significantly enhanced interface between perovskite and n-type material in active layer for efficient charge separation and enhanced power conversion efficiency (PCE). [6,6]-phenyl-C_{61}-butyric acid methyl ester ($PC_{61}BM$) is the most commonly used n-type materials in BHJ perovskite solar cells due to its high electron mobility. However, it is very difficult to fabricate BHJ perovskite films because of the poor solubility of $PC_{61}BM$ in commonly used solvent of dimethylformamide (DMF). In this study, we introduced two kinds of fluorinated-$PC_{61}BM$ (3F-$PC_{61}BM$ or 5F-$PC_{61}BM$) as n-type materials in the BHJ perovskite film, which have higher solubility in DMF than that of $PC_{61}BM$. Thus, the BHJ perovskite film can be easily fabricated by one-step using single solvent of BHJ precursor solution system for planar perovskite solar cell. The BHJ device of high PCE of 16.17% can be achieved by adding 0.1 wt% of 3F-$PC_{61}BM$ in perovskite precursor solution to fabricate solar cell, which is outperform than the PCE of 14.12% of pristine device. However, the addition of 5F-$PC_{61}BM$ decreases the PCE to be lower than that of the pristine device regardless its amount. We systematically study the effects of amount and type of fluorinated-$PC_{61}BM$ on the morphology of BHJ perovskite films using SEM, AFM, GISAXS and GIWAXS. The results reveal that 3F-$PC_{61}BM$ can fill the pinholes between perovskite grains and passivate the defects of pristine film. Thus, the current density (J_{sc}) is greatly increased. On the other hand, the self-aggregation of 5F-$PC_{61}BM$ in the BHJ perovskite films makes the films full with large voids, which lead to poor device performance. The dense and flat surface morphology of 3F-$PC_{61}BM$ containing perovskite BHJ films can also prevent the permeation of moisture into grain boundary and enhance the device stability. Therefore, the device can maintain 80% of original efficiency over 550 hours without any encapsulation as compared with the 240 hours of pristine device. Our results provide a novel strategy to fabricate high PCE and high stability BHJ perovskite solar cells for the realization of low cost solar cell in the near future.

Introduction

Recently organic-inorganic metal halide perovskites have become the promising materials in solar cell research due to their properties of long carrier diffusion length[1-6] and high absorption coefficient.[7-10] Nowadays, the highest certified power conversion efficiency (PCE) of the perovskite based solar cells is 22.1%.[11] There are three main kinds of device structures, including perovskite sensitized device,[8, 12-14] meso-superstructured device[15-17] and planar heterojunction (PHJ) device.[18-22] As compared with other two kinds of device, the PHJ device is investigated extensively because the whole device can be fabricated under low temperature of 150°C.[18, 20, 22] Many studies of PHJ solar cells report that the uniform perovskite film comprised of large crystal grains is closely related to the high PCE. Recently, the bulk heterojunction (BHJ) structure of fullerene derivative: perovskite blend film as the light absorption active layer attracts increased interest because of significantly enhanced photovoltaic performance.[23-28] This BHJ structure is fabricated by the perovskite blended with an appropriate amount of fullerene derivatives. The BHJ structure increases the interface between perovskite and fullerene derivative to form the network structure for efficient generation and transportation of charge carriers that results in enhanced PCE.

E. H. Sargent et al. first introduced [6,6]-phenyl-C_{61}-butyric acid methyl ester ($PC_{61}BM$) into perovskite solar cell to fabricate BHJ device. Due to poor solubility of $PC_{61}BM$ in dimethylformamide (DMF), which is commonly used solvent to dissolve perovskite precursor, they used the co-solvent process to solve this problem. They separately dissolved $PC_{61}BM$ in chlorobenzene and perovskite precursor in DMF. Then two solutions were mixed by high shear force to forcibly

[a] Department of Materials Science and Engineering, National Taiwan University, Taipei 10617, Taiwan. E-mail: suwf@ntu.edu.tw.
[b] Center of Condensed Matter Science, National Taiwan University, Taipei 10617, Taiwan.
[c] Institute of Nuclear Energy Research, Taoyuan 32546, Taiwan.
† These authors contributed equally to this work.
Electronic Supplementary Information (ESI) available: [details of any supplementary information available should be included here]. See DOI: 10.1039/x0xx00000x

disperse $PC_{61}BM$ in perovskite precursor. They showed that the BHJ devices made by this method can significantly reduce the hysteresis behavior and improve the PCE from 12.0% to 14.4%.[23] However, chlorobenzene is a poor solvent for perovskite,[29] a homogenous co-solvent system is difficult to achieve by just mixing two solutions of $PC_{61}BM$ /chlorobenzene and perovskite precursor/DMF. C. G. Wu et al. adopted a two-step process to fabricate the BHJ perovskite film.[24] They deposit a mixed solution of lead iodide and $PC_{71}BM$ in DMF to make a blending film (PbI_2:$PC_{71}BM$) first onto the substrate, followed by a second deposition of methanol ammonium iodide (MAI) in isopropyl alcohol to finish the transformation of perovskite. The $PC_{71}BM$ molecules can fill in the perovskite grain boundary and passivate the pinholes in the film by this method. However, $PC_{71}BM$ may hinder the diffusion of MAI to the bottom of PbI_2:$PC_{71}BM$ film. The transformation of underlying PbI_2 grains to perovskite would be restricted. The incomplete transformation active layer may limit the photovoltaic performance. Also, $PC_{71}BM$ is much more expensive than $PC_{61}BM$.

In order to increase the solubility of fullerene derivative in the perovskite precursor solution or enhance the stability of the BHJ device, some research groups tried to modify the fullerene to reach the goal. C. S. Hsu et al. utilized the cross-linkable $PC_{61}BM$ ([6,6]-phenyl-C_{61}-butyric styryl dendron ester, C-PCBSD) to improve the current density and stability of the BHJ device. They thermal annealed the BHJ perovskite film at 100°C for two to six hours for the transformation of perovskite and formation of the cross-linking C-PCBSD simultaneously.[25] However, long annealing time may not only cause the serious degradation of perovskite film but also waste energy. Recently, A. K. Y. Jen et al. incorporated fluoro-modified fullerene derivatives (DF-C_{60}) into BHJ film. The low surface energy of perfluorooctyl groups in DF-C_{60} makes this molecule preferably distributed nearby the surface region of the BHJ film. The hydrophobic surface of DF-C_{60} can prevent the permeation of moisture into the film, thus the stability of perovskite solar cell is improved.[26] However, the long fluorine carbon chains limit the solubility of DF-C_{60} in DMF. They also need to use co-solvent process to fabricate the BHJ perovskite film as mentioned above. In short summary, the BHJ perovskite solar cell tailored by the addition of fullerene derivative can be an effective way to increase the performance of solar cell. However, most of studies adopt co-solvent system[23, 26, 28] or other complex process,[24, 25, 27] which is difficult to control the quality of BHJ perovskite film. Also, no literature report discusses the detailed characteristics and the formation mechanisms of BHJ fullerene derivative: perovskite film. The mechanistic understanding of how the fullerene derivative molecules influence the morphology and the crystallization of perovskite phase related to the device performance is imperative but remains elusive at present time.

In this study, we show a novel strategy to significantly improve the PCE and long term stability of BHJ perovskite solar cell by using semi-fluorinated-$PC_{61}BM$. The trifluoroethyl or pentafluoropropyl groups are used to replace the methyl group on the side chain of $PC_{61}BM$ to make 3F-$PC_{61}BM$ and 5F-$PC_{61}BM$. With fluorinated modification, the solubility of $PC_{61}BM$ in perovskite precursor is improved significantly. Instead of complex fabricated process such as co-solvent or two-step process, we successfully fabricate the fluorinated-$PC_{61}BM$: perovskite BHJ perovskite solar cell by one-step and single solvent process. We systematically study the effects of amount and type of fluorinated-$PC_{61}BM$ on the morphology of BHJ perovskite films using scanning electron microscopy (SEM), atomic force microscopy (AFM), grazing incidence small- and wide-angle X-ray scattering (GISAXS and GIWAXS). The mechanism of perovskite film formation containing fluorinated-$PC_{61}BM$ is elucidated. The correlation between the film morphology and device performance is clearly resolved.

Experimental

Materials and Sample Preparation

The methylammonium iodide (MAI) was synthesized according to the literature.[22] Lead (II) acetate trihydrate ($Pb(Ac)_2{\cdot}3H_2O$, 99.999%, Aldrich) was dehydrated at 80°C in vacuum oven for 3 hours before used. The pristine perovskite precursor solution was prepared by mixing the MAI and dehydrated $Pb(Ac)_2$ with a 3:1 molar ratio in anhydrous N,N-dimethylformamide (DMF, 99.8%, Sigma-Aldrich). The solution concentration is 40 wt%. For the BHJ precursor solution, appropriated amount (from 0.1 wt% to 0.5 wt%) of 3F-$PC_{61}BM$ and 5F-$PC_{61}BM$ is directly incorporated into the perovskite precursor solution. All the precursor solutions are filtrated by 0.2 μm PTFE filter before further spin coating process.

The synthetic route for 3F-$PC_{61}BM$ and 5F-$PC_{61}BM$ are as following procedure. The [6, 6]-phenyl-C_{61}-butyric acid (PCBA) was obtained from PCBM by treating with hydrochloric acid and acetic acid in chlorobenzene reflux for 12h.[30] The mixture of PCBA (200 mg, 0.22 mmol) and 2,2,2-trifluoroethanol (44 mg, 0.44 mmol) was dissolved in 1,2-dichlorobenzene (100mL) and ultrasonicated for 2h, then cooled to 0 °C. Afterward, the dimethlylaminopyridine (DMAP) and dicyclohexylcarbodiimide (DCC) were added under N_2 atmosphere. The reaction mixture was stirred under N_2 at 0 °C for 30 min and allowed to stir at room temperature for 24h. The solvents were removed in high vacuum and the residue was precipitated by methanol. The crude product was purified by column chromatography using toluene/hexane (25:75) as the eluent to afford 3F-$PC_{61}BM$ in 67% yield. ^{1}H-NMR spectrum of 3F-$PC_{61}BM$ (400 MHz, $CDCl_3$, δ, ppm): 7.91-7.89 (m, 2H), 7.55-7.50 (m, 2H), 7.48-7.43 (m, 1H), 4.45 (q, 2H, J = 8.4 Hz), 2.92-2.88 (m, 2H), 2.61 (t, 2H, J = 7.6 Hz), 2.23-2.15 (m, 2H). ^{19}F NMR (376.5 MHz, $CDCl_3$, δ, ppm): -73.59 (t, J = 8.65 Hz, 3F). ^{13}C-NMR (100 MHz, $CDCl_3$, δ, ppm) : 171.3, 148.7, 147.6, 145.8, 145.2, 145.1, 145.0, 144.7, 144.6, 144.5, 144.4, 143.9, 143.7,143.1,143.0, 142.9, 142.9, 142.2, 142.1, 142.1, 140.9, 140.7, 138.0, 137.5, 136.5, 132.0, 128.5, 128.3, 124.2, 121.5, 79.7, 60.3 (q, J = 36.3 Hz), 51.6, 33.5, 33.3, 22.0. MALDI-TOF-MS m/z: calculated for $C_{73}H_{13}O_2F_3$ 978.09, found 977.96 (M^+).

The synthetic procedure of 5F-$PC_{61}BM$ was similar to that of 3F-$PC_{61}BM$. Reaction of PCBA (200 mg, 0.22 mmol) and

View Article Online
DOI: 10.1039/C7TA07970C

2,2,3,3,3-pentafluoro-1-propanol (67 mg, 0.44 mmol) to afford 5F-$PC_{61}BM$ in 59 % yield. ^{1}H NMR spectrum of 5F-$PC_{61}BM$ (400 MHz, $CDCl_3$, δ, ppm): 7.91-7.88 (m, 2H), 7.55-7.51 (m, 2H), 7.48-7.44 (m, 1H), 4.56-4.49 (m, 2H), 2.92-2.88 (m, 2H), 2.60 (t, 2H, J = 7.6 Hz), 2.23-2.15 (m, 2H). ^{19}F NMR (376.5 MHz, $CDCl_3$, δ, ppm): -83.72, -123.33. ^{13}C NMR (100 MHz, $CDCl_3$, δ, ppm) :171.3, 148.7, 147.6, 145.8, 145.2, 145.0, 144.8, 144.7, 144.6, 144.5, 144.4, 144.0, 143.7, 143.1, 143.0, 142.9, 142.9, 142.2, 142.1, 142.1, 141.0, 140.7, 138.0, 137.5, 136.5, 132.0, 128.5, 128.3, 79.7, 59.1 (t, J = 27.4 Hz), 51.6, 33.5, 33.4, 22.0. MALDI-TOF-MS m/z: calculated for $C_{74}H_{13}O_2F_5$ 1028.08, found 1028.08 (M^+).

Fabrication of the perovskite solar cell

Our BHJ perovskite solar cells have the structure of ITO/PEDOT:PSS/fluorinated-$PC_{61}BM$: perovskite/$PC_{61}BM$/PEI/Au. The fabrication procedure is as following. First, the ITO substrate (Buwon, 10Ω) was cleaned sequentially by ammonium/hydrogen peroxide/deionized water, methanol, isopropanol and 15 minutes oxygen plasma treatment. Next, the PEDOT:PSS was spin coated on the as-cleaned ITO substrate by 3000 rpm for 30 seconds followed by baking at 140°C for 20 minutes to form the hole transporting layer. The ITO/PEDOT:PSS substrates were then transferred into a nitrogen atmosphere glove box and the as-prepared precursor solutions were spin coated over by 2000 rpm 40 seconds. The films were subsequently thermal annealing at 100°C for 3 minutes to form the photoactive layer. Afterwards, the $PC_{61}BM$ solution (20mg in 1 ml chlorobenzene) was spin coated over the photoactive layer with 1000 rpm for 30 seconds to serve as electron transporting layer. Finally, the PEI interface modified layer and the gold electrode with the thickness of 100nm were deposited on the top of device to finish the fabrication of BHJ perovskite solar cells.

Characterization

For the photoelectronic performance characterization, the devices were exposed under the AM 1.5G solar simulator (Newport, 69920) with 100 $mWcm^{-2}$ irradiation intensity and recorded the J-V curves by using voltage source meter (Keithley 2410). The PL spectra were measured with a continuous-wave diode laser source (PDLH-440-25, DongWoo Optron Co. Ltd.) and detected the emission spectra by a photomultiplier tube detector system (PDS-1, DongWoo Optron Co. Ltd.). The TRPL spectra were measured by a time-correlated single photon counting spectrometer (WELLS-001 FX, DongWoo Optron Co. Ltd.). The pulse laser with 440nm wavelength has the average power of 1 mW and operated with 2 μs excitation duration. The surface morphologies of BHJ film were observed by the field emission SEM (JSM-6700F, JOEL) at an accelerating voltage of 10 kV. The surface height information was obtained by the AFM (OMV-NTSC, Bruker). The simultaneously synchrotron GISAXS/GIWAXS measurements were performed at the beam line 23A of the National Synchrotron Radiation Research Center (NSRRC), Taiwan. The pristine or BHJ perovskite film were as-spin coat on the Si/PEDOT:PSS substrates. The monochromated X-ray beam with wavelength of 1.24 Å and 0.20° incidence angle was applied to characterize the film. The sample-to-detector distance of GISAXS and GIWAXS measurement were 461.1 cm and 14.3 cm, respectively. The 1D GISAXS profiles were obtained by line integrated the 2D GISAXS patterns along the in-plane direction. The water contact angle measurements were performed by a contact angle goniometer (model 100SB, Sindatek Instrument Co. Ltd.).

Results and Discussion

We adopted the p-i-n device structure of ITO/PEDOT:PSS/fluorinated-$PC_{61}BM$: perovskite/$PC_{61}BM$/PEI/Au to fabricate the BHJ perovskite solar cells. Two strategies of material synthesis are applied to obtain high quality BHJ perovskite film. The first one is using lead acetate ($Pb(Ac)_2$) as lead source of perovskite.[31] The transition process of $Pb(Ac)_2$ with MAI to perovskite is described as below:

$$Pb(Ac)_2+3CH_3NH_3I \rightarrow CH_3NH_3PbI_3+2CH_3NH_3(Ac) \uparrow \quad (Ac = CH_3COO)$$

Note that the by-product $CH_3NH_3(Ac)$ is thermally unstable and is easily to be evaporated during the thermal annealing process. That forces the reaction toward right and accelerates the formation of perovskite. Using lead acetate and MAI as perovskite precursor materials can simplify the fabrication process of BHJ film at 100°C for only 5 minutes. The second strategy is using fluorinated-$PC_{61}BM$ as n-type materials in the BHJ perovskite film. Fig. 1 (a) and Fig. 1 (b) shows the molecular structure of 3F-$PC_{61}BM$ and 5F-$PC_{61}BM$, respectively, where the methyl group on the side chain of $PC_{61}BM$ is replaced by different length of fluoroalkyl chain. The 3F-$PC_{61}BM$ and 5F-$PC_{61}BM$ are synthesized through the esterification of [6, 6]-phenyl-C_{61}-butyric acid (PCBA) by 2,2,2-trifluoroethanol and 2,2,3,3,3-pentafluoro-1-propanol respectively, as shown in Scheme 1. The chemical structures of synthesized compounds are confirmed by ^{1}H-NMR, ^{13}C-NMR, ^{19}F-NMR and mass spectroscopy (see details in experimental section). The fluoroalkyl groups can increase the molecular polarity and improve the solubility in DMF. The measured solubility 3F-$PC_{61}BM$, 5F-$PC_{61}BM$ in DMF are 4.0 mg/ 1mL and 2.5 mg/ 1mL, respectively, which are twenty and twelve times higher than that of $PC_{61}BM$ (0.2 mg/ 1mL). It is worth to note the low molecular polarity of pentafluoropropyl group would make the solubility of 5F-$PC_{61}BM$ in DMF lower than that of 3F-$PC_{61}BM$. Nevertheless, we can still blend fluorinated-$PC_{61}BM$, lead acetate and MAI all in DMF as precursor solution to fabricate the BHJ light absorption active layer by a one-step and single solvent process.

Before going to fabricate the BHJ perovskite solar cells, we need to carefully characterize the optical and electronic properties of 3F-$PC_{61}BM$ and 5F-$PC_{61}BM$ to ensure they are suitable materials for the BHJ perovskite films. The space charge limited current (SCLC) model was performed to calculate the electron mobility of $PC_{61}BM$, 3F-$PC_{61}BM$ and 5F-$PC_{61}BM$. The data are shown in the supporting information. Fig.

View Article Online
DOI: 10.1039/C7TA07858C

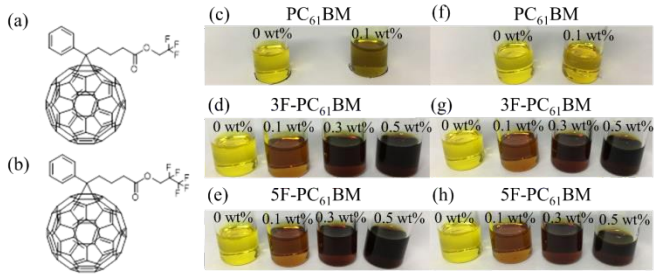

Fig. 1 Chemical structures of (a) 3F-$PC_{61}BM$ and (b) 5F-$PC_{61}BM$. Photos of BHJ perovskite precursor solutions containing different concentration of $PC_{61}BM$, 3F-$PC_{61}BM$, 5F-$PC_{61}BM$: (c)-(e) without filtration and (f)-(h) with filtration.

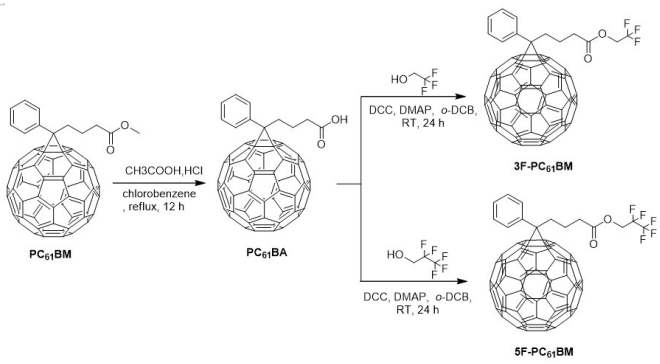

Scheme 1 Chemical reactions of 3F-$PC_{61}BM$ and 5F-$PC_{61}BM$ syntheses.

S1 (a) shows the cell architecture. Fig. S1 (b) indicates measured current density-effective voltages curves and the results are summarized in Table S1. The electron mobility of $PC_{61}BM$, 3F-$PC_{61}BM$ and 5F-$PC_{61}BM$ are estimated to be 4.16×10^{-4} $cm^2V^{-1}s^{-1}$, 5.61×10^{-4} $cm^2V^{-1}s^{-1}$ and 2.69×10^{-4} $cm^2V^{-1}s^{-1}$, respectively. The slight decrease in electron mobility of 5F-$PC_{61}BM$ molecules may be resulted from the poor molecular packing of bulky pentafluoropropyl group. However, all of the mobility of fluorinated-$PC_{61}BM$ are still in the same order of 10^{-4} $cm^2V^{-1}s^{-1}$ as that of $PC_{61}BM$. It indicates that fluorinated-$PC_{61}BM$ still has comparable ability to transport electrons.

Besides the carrier mobility of fluorinated-$PC_{61}BM$, we also need to ensure the energy levels of fluorinated-$PC_{61}BM$ are adequate for the BHJ device. The combined cyclic voltammograms (CV) and ultraviolet-visible absorption spectra (UV-vis) measurements were carried out to determine the lowest unoccupied molecular orbital (LUMO) and highest occupied molecular orbital (HOMO) of fluorinated-$PC_{61}BM$, as shown in Fig. S2 (a) and Fig. S2 (b). The calculated energy levels are listed in Table S2. The LUMO levels of $PC_{61}BM$, 3F-$PC_{61}BM$ and 5F-$PC_{61}BM$ were determined by the following equation: $E_{LUMO} = -e[E_{red}^{onset} + 4.6]$ and the E_{red}^{onset} is the reduction potential for sample. The HOMO levels are estimated by subtracted the LUMO levels from the values of band gap, which are derived from UV-vis absorption spectra. Both HOMO and LUMO levels of 3F-$PC_{61}BM$ and 5F-$PC_{61}BM$ are lower than the energy levels of $PC_{61}BM$ by 0.2 eV. This is due to the presences of strong electron withdrawing fluoroalkyl group in fluorinated-$PC_{61}BM$ which makes fluorinated-$PC_{61}BM$ become more electron-deficient. Thus, the fluorinated-$PC_{61}BM$ exhibits a negative shift of energy level from that of pristine $PC_{61}BM$. The band diagram of our BHJ device is shown in Fig. S2 (c). The build-in potential of the BHJ absorption layer is still suitable for excitons to be separated. There is also no energy barrier in BHJ band diagram to block the transport of electrons or holes from light absorption layer to counter electrodes. In short summary, the fluoroalkyl group in fluorinated-$PC_{61}BM$ can modify fluorinated-$PC_{61}BM$ to have higher solubility than $PC_{61}BM$ without sacrificing the optical and electrical properties.

After the characterization of basic properties of materials, we blended different amount of either 3F-$PC_{61}BM$ or 5F-$PC_{61}BM$ (based on perovskite weight) into perovskite precursor to prepare the BHJ precursor solutions. Fig. 1 (c) - (e) are photos of our BHJ precursor solutions without filtration. Fig. 1 (c) compares the difference of solution appearance between the pristine perovskite precursor solution and BHJ precursor solution containing 0.1 wt% $PC_{61}BM$. Due to the poor solubility of $PC_{61}BM$ in DMF, there are many insoluble aggregations in BHJ precursor solution, which make the solution turbid. However, for the BHJ precursor solutions blended with 3F-$PC_{61}BM$ and 5F-$PC_{61}BM$, as shown in Fig. 1 (d) and Fig. 1 (e), all the BHJ precursor solutions stay transparent even at high concentration of 0.5 wt% 3F-$PC_{61}BM$ and 5F-$PC_{61}BM$. By filtration, almost all insoluble aggregations in 0.1 wt% $PC_{61}BM$: perovskite BHJ precursor solution are removed and its color is close to that of perovskite solution, as shown in Fig. 1 (f). On the other hand, there is no color change after the filtration for BHJ precursor solutions containing 3F-$PC_{61}BM$ and 5F-$PC_{61}BM$, as shown in Fig. 1 (g) and Fig. 1 (h). Thus, 3F-$PC_{61}BM$ and 5F-$PC_{61}BM$ can be homogeneously dispersed in perovskite precursor solution and are suitable to fabricate BHJ perovskite solar cells.

To explore the optimized concentration of 3F-$PC_{61}BM$ and 5F-$PC_{61}BM$ in perovskite precursor solution for the fabrication of devices, we varied their concentrations from 0.05 wt% to 0.5 wt%. The measured current density-voltage (J-V) curves of fluorinated-$PC_{61}BM$: perovskite BHJ devices are shown in Fig. S3 and their corresponding photovoltaic parameters are summarized in Table S3 and Table S4, respectively. The pristine device exhibits PCE of 14.12% with open circuit voltage (V_{oc}) of 1.01 V, short circuit current density (J_{sc}) of 19.96 mA cm^{-2} and fill factor (FF) of 71.10 %. By the incorporation of 0.05 wt% 3F-$PC_{61}BM$, there is almost no performance difference between pristine device and BHJ device. Therefore, we further increase the concentration of 3F-$PC_{61}BM$ to 0.1 wt%. The performance can be significantly improved and show a PCE of 16.17%, with V_{oc} of 1.00 V, J_{sc} of 21.78 mA cm^{-2}, FF of 73.34%. However, as the concentration of 3F-$PC_{61}BM$ in BHJ film further increased to over 0.1 wt%, the performance of BHJ devices starts to decrease, as shown by the PCE of 13.58% and 12.67% when the blending amounts of 0.3wt% and 0.5wt% of 3F-$PC_{61}BM$ are used, respectively. On the other hand, for 5F-$PC_{61}BM$: perovskite BHJ devices, no matter what is its concentration in BHJ films, the performance of BHJ devices are always worse than that of pristine device. In order to study how the number

of fluorine atoms affects the performance of BHJ devices, we fix the concentration of fluorinated-$PC_{61}BM$ at 0.1 wt% in perovskite layer and compare the device performance with the pristine device. We fabricated 15 devices for each kind of perovskite composition, their photovoltaic performances were evaluated and the standard deviations were calculated. The J-V curves and performance of these three type devices are summarized in Fig. 2 and Table 1. The data show the amount increase in average PCE for 0.1 wt%, 3F-$PC_{61}BM$ device as compared with the pristine device is statistically significant. At the same concentration of 0.1 wt%, 3F-$PC_{61}BM$ molecules can effectively improve the J_{sc} and PCE from 19.96 mA cm^{-2} and 14.12% of pristine device to 21.78 mA cm^{-2} and 16.17%, respectively, while 5F-PC61BM molecules cause the dramatic decrease of V_{oc} to 0.87 V, J_{sc} to 14.99 mA cm^{-2}, FF to 65.71% and the PCE to 8.65%. It can be concluded that the performance of BHJ devices are highly related to the fluoroalkyl chain length in fluorinated-$PC_{61}BM$. We therefore investigate how the fluorinated-$PC_{61}BM$ affects the properties of BHJ films by optical and morphological studies.

We first analyzed the difference of carrier extraction efficiency between pristine perovskite film and 0.1 wt% fluorinated-$PC_{61}BM$: perovskite BHJ films using photoluminescence (PL) spectroscopy as represent in Fig. 3 (a). A significant intensity quenching in the PL intensity is observed for the BHJ perovskite films. It illustrates that incorporating fluorinated-$PC_{61}BM$ into light absorption layer can increase the amount of heterojunction between perovskite and fluorinated-$PC_{61}BM$. The extraction of photo-generated excitons is more effectively that reduces the possibility of recombination. Thus, the time-resolved photoluminescence (TRPL) measurement was used to probe the ability of charge dissociation in the pristine perovskite film and 0.1 wt% fluorinated-$PC_{61}BM$: perovskite BHJ films, as shown in Fig. 3 (b). The related parameters are summarized in Table 2. All of the exponential decay profiles are fitted by the bi-exponential model ($I(t) = A_1 e^{-t/\tau_1} + A_2 e^{-t/\tau_2}$) which contains charge transfer mechanism (fraction A_1, time for charge transfer τ_1) and radiative decay mechanism (fraction A_2, time for radiative decay τ_2).[32] Here, the charge transfer is the dominant mechanism to affect the decay of intensity. We thus put emphasis on the required time for charge transfer and its fraction. For the pristine perovskite film, the time of charge transfer is 24.16 ns and the fraction of charge transfer is 88%. By blending 0.1 wt% 3F-$PC_{61}BM$ into perovskite film, the required time for charge transfer decreases from 24.16 ns to 4.72 ns, and the fraction can be increased from 88% to 99%. It means that once the excitons are generated by incident light in perovskite material, they can be very efficiently separated. In addition, blending 0.1 wt% 5F-$PC_{61}BM$ into perovskite film can also decrease the required time of charge transfer to 5.93 ns and increase the fraction to 99%. Although BHJ film blended with 0.1 wt% 5F-$PC_{61}BM$ has better ability to transfer carriers in comparison with pristine perovskite film, all the performance parameters of 0.1 wt% 5F-$PC_{61}BM$: perovskite BHJ device performance are worse than that of pristine device. It motivates us to do in depth analysis on the morphology of BHJ perovskite film, so one can understand the effect of fluorinated-$PC_{61}BM$ on the performance of BHJ devices.

The SEM is employed to analyze the surface morphology of BHJ perovskite film. Fig. 4 shows the top-view SEM images of pristine perovskite film and 0.1 wt% fluorinated-$PC_{61}BM$: perovskite BHJ films on the substrate of ITO/PEDOT:PSS. The SEM images of BHJ perovskite films containing different concentration of fluorinated-$PC_{61}BM$ are shown in Fig. S4. The pristine perovskite film consists of many small grains, which distributes randomly and results in relatively rough surface (Fig. 4 (a)). For the 0.1 wt% 3F-$PC_{61}BM$: perovskite BHJ film, its surface becomes smoother than that of pristine perovskite film. The 3F-$PC_{61}BM$ homogeneously dispersed in the grain boundaries of perovskite passivate the defects and form a smooth film (Fig. 4 (b)), which can improve the contact between perovskite film and electron transporting layer.

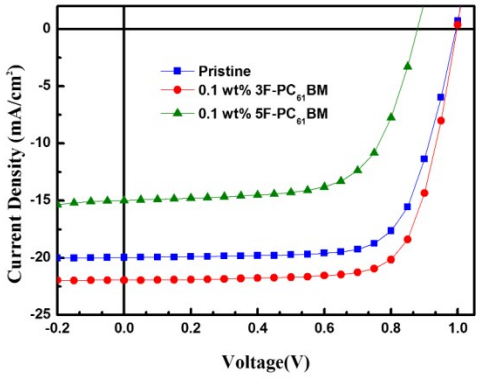

Fig. 2 J-V curves of pristine device and BHJ devices blended with 0.1 wt% 3F-$PC_{61}BM$ and 0.1 wt% 5F-$PC_{61}BM$.

Table 1 Device performance of BHJ perovskite solar cells containing different amount of fluorinated-$PC_{61}BM$.

Device	V_{oc} (V)	J_{sc} (mA cm^{-2})	FF (%)	PCE (%)
0 wt%	1.01	19.96	71.10	14.12 (13.36 ± 0.64)
0.1 wt% 3F-$PC_{61}BM$	1.00	21.78	73.34	16.17 (14.93 ± 0.71)
0.1 wt% 5F-$PC_{61}BM$	0.87	14.99	65.71	8.65 (7.66 ± 1.02)

View Article Online
DOI: 10.1039/C7TA07939G

Table 2 Fitting results of time-resolved photoluminescence characterization.

Sample	τ_1 (ns)	Fraction (%)	τ_2 (ns)	Fraction (%)	$\tau_{Average}$ (ns)
$CH_3NH_3PbI_3$	24.16	88	56.69	12	28.12
$CH_3NH_3PbI_3$:0.1 wt% 3F-$PC_{61}BM$	4.72	99	18.23	1*	4.73
$CH_3NH_3PbI_3$:0.1 wt% 5F-$PC_{61}BM$	5.93	99	20.65	1*	6.07

* In these cases, the radiative decay contribution is certainly not larger than the error of the experiment.

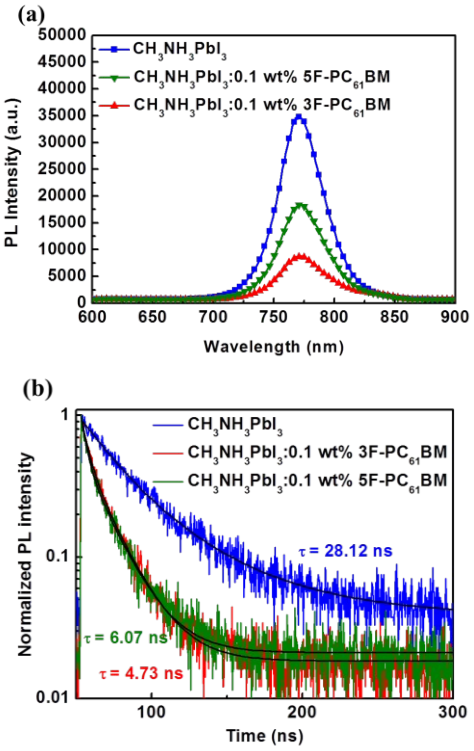

Fig. 3 (a) Photoluminescence spectra of pristine perovskite film, 0.1 wt% 3F-$PC_{61}BM$: perovskite and 0.1 wt% 5F-$PC_{61}BM$: perovskite BHJ films. (b) Time-resolved photoluminescence characterization of pristine perovskite film, 0.1 wt% 3F-$PC_{61}BM$: perovskite and 0.1 wt% 5F-$PC_{61}BM$: perovskite BHJ films.

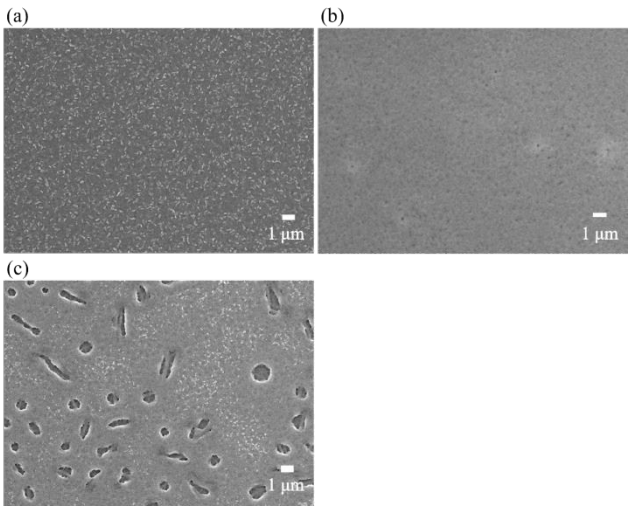

Fig. 4 SEM images of (a) pristine perovskite film (b) 0.1 wt% 3F-$PC_{61}BM$: perovskite BHJ film (c) 0.1 wt% 5F-$PC_{61}BM$: perovskite BHJ film.

Moreover, the incorporated 3F-$PC_{61}BM$ can effectively separate the excitons and extracts charges from perovskite, so J_{sc} and PCE can be increased and outperform that of pristine device. When we increased the concentration of 3F-$PC_{61}BM$ from 0.1 wt% to 0.5 wt%, there are some aggregated clusters on the surface of film (Fig. S4 (a) and (b)). That is due to the low surface energy property of 3F-$PC_{61}BM$ molecules which undergoes phase separation and forms aggregates and voids at higher concentration in BHJ films. Thus, the PCE of BHJ device is decreased from 16.17% to 12.67% at 0.5 wt% 3F-$PC_{61}BM$ (Table S3). On the other hand, for the BHJ perovskite film containing 0.1 wt% 5F-$PC_{61}BM$, many big holes with over one micrometer diameter are observed in the film, as shown in Fig. 4 (c). The low surface energy property of 5F-$PC_{61}BM$ is not compatible with perovskite that results in self-aggregation to obstruct the formation of continuous film. The present of holes in the film leads to the direct contact between electron transporting layer and hole transporting layer that dramatically decreases the performance of BHJ devices. Therefore, the device shows poor PCE of only 8.65%. Further increasing the amount of 5F-$PC_{61}BM$ leads to the over-coalescence of perovskite grains with large voids and even strip like grains, as shown in Fig. S4 (c) and (d). The PCE of BHJ device dramatically dropped to 4.30% at 0.5 wt% 5F-$PC_{61}BM$ (Table S4).

The morphology of BHJ films is further studied by AFM to visualize the roughness and depth profile of the as-deposited films. Fig. 5 shows the AFM topography and depth information of pristine perovskite film and 0.1 wt% fluorinated-$PC_{61}BM$: perovskite BHJ films. The AFM topography of 0.3 wt% and 0.5 wt% of fluorinated-$PC_{61}BM$: perovskite BHJ films are shown in Fig. S5 and Fig. S6. The pristine perovskite film with small disorder grains shows the root mean square roughness (RMS) of 16.90 nm (Fig. 5 (a)). The addition of 0.1 wt% 3F-$PC_{61}BM$ into perovskite film (Fig. 5 (b)) could make the RMS significantly reduced to 8.33 nm. We speculate that 3F-$PC_{61}BM$ fills the defects of perovskite and makes the film smoother. The causes of increased smoothness are investigated by GISAXS and GIWAXS. The results will be discussed in details in the next section. The improved morphology of 0.1 wt% 3F-$PC_{61}BM$: perovskite film enhances the PCE of device from 14.12% to 16.17%. On the contrary, the BHJ perovskite film containing 0.1 wt% 5F-$PC_{61}BM$ has the RMS of 64.90 nm (Fig. 5 (c)). The holes in the film are deep enough for direct contact between electron transporting layer and hole transporting layer, so the 0.1 wt% 5F-$PC_{61}BM$: perovskite BHJ device exhibits poor PCE of 8.65%. As the concentration of 3F-$PC_{61}BM$ increase to 0.3 wt% or 0.5 wt%, although the RMS value of 3F-

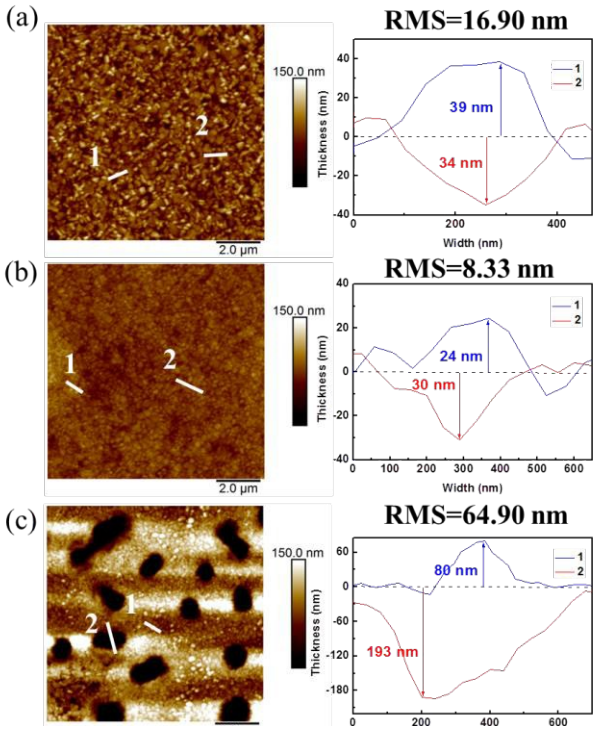

Fig. 5 AFM surface height images and depth information of (a) pristine perovskite film (b) 0.1 wt% 3F-PC_{61}BM: perovskite BHJ film (c) 0.1 wt% 5F-PC_{61}BM: perovskite BHJ film.

PC_{61}BM: perovskite BHJ films are still lower than pristine perovskite film, the aggregated clusters on the surface of the BHJ perovskite films gradually grow, as shown in Fig. S5. The aggregated clusters render a poor contact between BHJ film and electron transporting layer. Thus, the device performance decreases with increasing the concentration of 3F-PC_{61}BM. The surface roughness of 5F-PC_{61}BM: perovskite BHJ films increases further when the concentration of 5F-PC_{61}BM increases to 0.3 wt% and 0.5 wt% (Fig. S6). The depth of voids can be as large as 239 and 260 nm for 0.3 wt% and 0.5 wt% 5F-PC_{61}BM: perovskite BHJ films, respectively. Thus, the PCE of 0.3 wt% and 0.5 wt% 5F-PC_{61}BM: perovskite BHJ devices are decreased to 5.82% and 4.30% respectively from 8.65% of 0.1 wt% 5F-PC_{61}BM: perovskite BHJ devices.

The study of surface morphology by SEM and AFM is limited to a very local and small area. We employed simultaneously synchrotron GISAXS/GIWAXS measurements to investigate the detailed bulk morphology of the fluorinated-PC_{61}BM: perovskite BHJ films. Fig. 6 (a) shows the GISAXS profiles of pristine perovskite film and the BHJ films contained 0.1, 0.3 and 0.5 wt% 3F-PC_{61}BM. The GISAXS profiles of all BHJ films show the behavior of power-law scattering ($I(Q) \propto Q^{-\alpha}$) in the Q region of 0.005~0.05 Å^{-1}. Here, the exponent α is related to the fractal dimension D, where $D = 6 - \alpha$.[33] The D of the pristine perovskite film and the 3F-PC_{61}BM BHJ films are summarized in Table 3. The D of BHJ films is between 2 to 3, which reveal the characteristic of surface fractal. The surface fractal indicates the films have the two dimensional (2D) self-similar morphology at different scales from nanometers to micrometers. It implies the internal structures of films are comprised of densely packed perovskite grains. Note that the D values decrease as the amount of 3F-PC_{61}BM increases, which means the addition of 3F-PC_{61}BM molecules can induce the packing of perovskite grains to form a dense film. However, the excess amount of 3F-PC_{61}BM (over 0.1 wt%) induces phase separation, thus forms self-aggregate clusters and voids on the surface and bulk of BHJ film, as observed in the SEM images (Fig. S4) and AFM images (Fig. S5), which render poor contact between BHJ film and electron transporting layer. As a result, the device performance decreased. In contrast to the BHJ films, the GISAXS profile of the pristine perovskite film shows a similar power-law scattering characteristic except a weak shoulder in the middle Q region of 0.009~0.03 Å^{-1} (Fig. 6 (a) inset). Thus, the pristine perovskite film mainly has the characteristic of pore structure. It can be concluded that the incorporation of 3F-PC_{61}BM molecules could significantly influence the formation behavior and structure of perovskite film, including the bulk and surface morphologies. The schematic illustration for formation of BHJ film containing 3F-PC_{61}BM is shown in Fig. 7 (a). At an appropriated amount (0.1 wt%), the 3F-PC_{61}BM can disperse well in the perovskite precursor solution and help the nucleation and growth of perovskite grains into the densely-packed film.

The GISAXS profiles of BHJ films contained 0.1, 0.3 and 0.5 wt% 5F-PC_{61}BM are shown in Fig. 6 (b). All GISAXS profiles show the behavior of power-law scattering in the low Q range (0.005 ~ 0.02 Å^{-1}). The values of fractal dimension Q are between 3 to 4, which indicates all 5F-PC_{61}BM: perovskite BHJ films have the characteristic of mass fractal. The mass fractal morphology is comprised by the fractal network structure formed from the aggregation of primary particles. Therefore, in order to fit the GISAXS profiles in the whole Q range well, the fitting model needs to contain the form factor $P(Q)$ of the primary particles and the structure factor $S(Q)$ of mass fractal network. The model fitting profile can be expressed as following equation:

$$I(Q) = P(Q)S(Q) \quad (1)$$

From previous report, we know that the primary particle in the mass fractal perovskite film has the pore-like structure.[33] The $P(Q)$ calculation considers the mean radius R of the primary pore with a standard deviation size distribution polydispersity, p. The $S(Q)$ describes the interaction between primary pores in the mass fractal network system, which is expressed as below:

$$S(Q) = 1 + \frac{\sin[(D-1)+\tan^{-1}(Q\xi)]}{(QR)^{D}} \cdot \frac{D\Gamma(D-1)}{[1+1/(Q\xi)^2]^{(D-1)/2}} \quad (2)$$

where ξ is the correlation length of the fractal pore network system, which denotes the distance between the aggregation of primary pores. D_p is the mass fractal dimension, $\Gamma(D_p - 1)$ is the gamma function of the variable $(D_p - 1)$. The fitted parameters about the fractal pore network in the perovskite grain or between the grains boundary are listed Table 4.

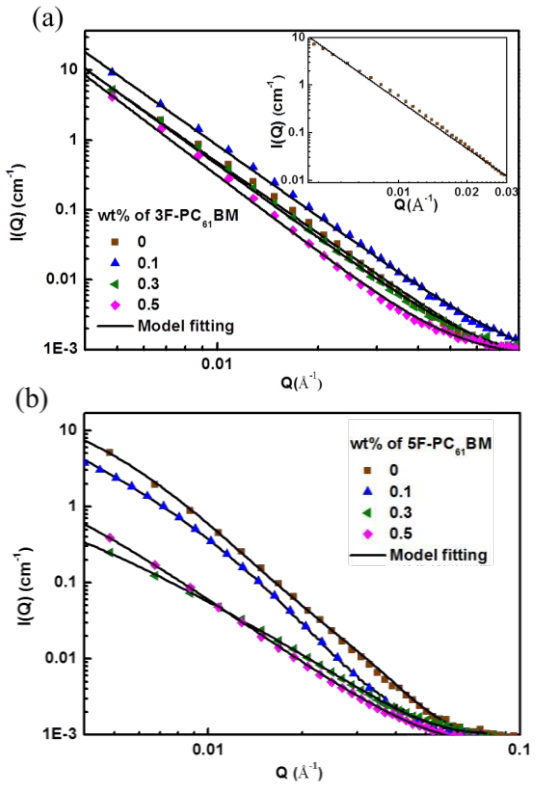

Fig. 6 (a) GISAXS profiles of BHJ perovskite films made from different concentration of 3F-PC$_{61}$BM. The solid lines are calculated by power-law model and the inset figure is the magnification of pristine film profile in middle *Q* range to show the mismatch between raw data and model fitting. (b) GISAXS profiles of BHJ perovskite films made from different concentration of 5F-PC$_{61}$BM. The solid lines are calculated by fractal poly-sphere model.

Table 3 Structural parameters determined by the power-law model fitting for the BHJ perovskite films blended with different concentration of 3F-PC$_{61}$BM using GISAXS spectroscopy.

wt% of 3F-PC$_{61}$BM in active layer	Fractal type	*D*
0	Pore	2.95*
0.1	Surface	2.63
0.3	Surface	2.53
0.5	Surface	2.38

*The power-law cannot fit the 0 wt% perovskite film GISAXS profile well.

Table 3 Structural parameters determined by fractal poly-sphere model fitting for the BHJ perovskite films blended with different concentration of 5F-PC$_{61}$BM using GISAXS spectroscopy.

wt% of 5F-PC$_{61}$BM in active layer	Fractal type	*R* (nm)	D_p	*p*	ζ (nm)
0	Pore	4.9	2.95	0.4	24
0.1	Pore	3.7	2.71	0.6	25
0.3	Pore	2.6	2.18	0.5	40
0.5	Pore	2.8	2.55	0.4	41

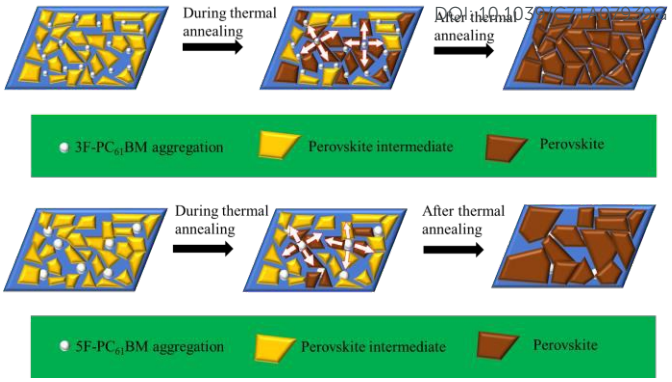

Fig. 7 Schematic illustrations for the formation mechanism of BHJ film containing (a) 3F-PC$_{61}$BM and (b) 5F-PC$_{61}$BM.

The fitting results show that the polydisperse primary pores in the pristine perovskite film have the mean radius of 4.9 nm with ~24 nm correlation length. As adding 0.1 wt% of 5F-PC$_{61}$BM into the film, the pore size shrinks to 3.7 nm with slightly increase in correlation length to ~25 nm. The radius of primary pore further decreases to ~2.8 nm and the correlation length of fractal domains grows to ~40 nm when the amount increases to 0.3 or 0.5 wt%. The change of the pore size and the correlation length with different amount of 5F-PC$_{61}$BM can be used to explain the morphology changes observed in the studies of SEM and AFM. We speculate that 5F-PC$_{61}$BM molecules in the perovskite could substantially aggregate even though the amount is low. The schematic illustration for formation of BHJ film containing 5F-PC$_{61}$BM is shown in Fig. 7 (b). As the amount of 5F-PC$_{61}$BM in the film increases, the large aggregation behavior leads to heterogeneous nucleation and growth of perovskite crystallites followed by the over-coalescence of grains with large voids and even strip like grains.

Fig. 8 shows the 2D GIWAXS patterns of the pristine perovskite film and the BHJ films containing 0.1 wt% fluorinated-PC$_{61}$BM. All the films display the prefer orientation of perovskite crystallites with the diffraction spot of (110) plane in the out-of-plane direction (normal to the film or substrate surface). The calculated perovskite crystal sizes are all about 40 nm. Among of them, the 3F-PC$_{61}$BM: perovskite BHJ films exhibits the highest diffraction intensity of (110) plane. The homogeneously dispersed of 3F-PC$_{61}$BM in the grain boundaries could restrict the lateral growth of perovskite grains, which promote the densely packing of perovskite grains and growth in out-of-plane direction. The improvement of the perovskite out-of-plane direction crystallinity is benefit to the charge transportation in the perovskite solar cells. In contrast, the substantial aggregations of 5F-PC$_{61}$BM molecules are hard to be homogeneously dispersed in the perovskite grain boundaries. The lateral growth of perovskite grains is not restricted in this case. Therefore, the 5F-PC$_{61}$BM: perovskite BHJ films exhibits the lowest diffraction intensity of (110) plane in the out-of-plane direction among all the films.

Finally, Fig. 9 (a) compares the stability of pristine device and 0.1 wt% 3F-PC$_{61}$BM: perovskite BHJ device. These devices were stored in a nitrogen filled glove box without

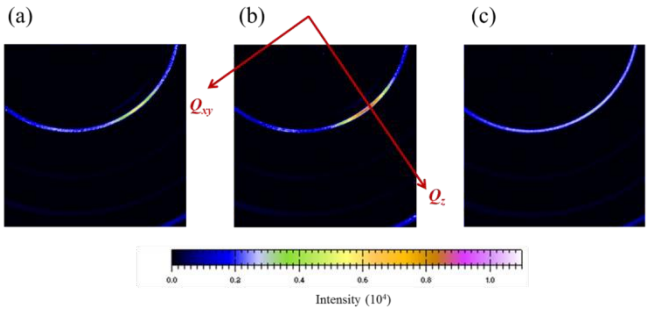

Fig. 8 Two dimensional (2D) GIWAXS patterns of (a) pristine $CH_3NH_3PbI_3$ (b) 0.1 wt% 3F-PC_{61}BM: $CH_3NH_3PbI_3$ and (c) 0.1 wt% 5F-PC_{61}BM: $CH_3NH_3PbI_3$ BHJ films. Q_z and Q_{xy} directions are the out-of-plane and in-plane directions, respectively.

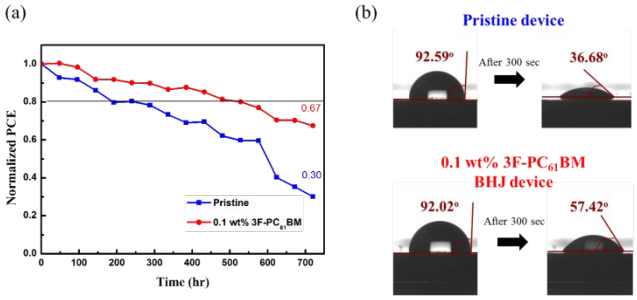

Fig. 9(a) Stability measurement of pristine and 0.1 wt% 3F-PC_{61}BM: perovskite BHJ solar cells. (b) Contact angle measurements for pristine perovskite device and 0.1 wt% 3F-PC_{61}BM: perovskite BHJ device conducted at 0 sec and 300 sec.

encapsulation. Then they were taken out the glove box periodically and measured the device performance in ambient (25°C/50% relative humidity). The PCE of pristine perovskite solar cell degrades to 80% of original performance after only 240 hours storage. However, the PCE of 0.1 wt% 3F-PC_{61}BM: perovskite BHJ device can maintain 80% of original efficiency over 550 hours. We also performed the water contact angle measurements on pristine device and 0.1 wt% 3F-PC_{61}BM: perovskite BHJ device at the area without electrode, as shown in Fig. 9 (b). Initially, these two devices have similar water contact angle about 92°. After 5 mins, the water contact angle of 0.1 wt% 3F-PC_{61}BM: perovskite BHJ device become 57.42°, which is higher than that of pristine device at 36.68°. This difference in water contact angle is due to the difference in film morphology. The BHJ film containing 0.1 wt% 3F-PC_{61}BM had a flat and less pinhole film, which can prevent the invasion of moisture into perovskite grain boundaries. The results indicate that the incorporation of 3F-PC_{61}BM can indeed improve the stability of BHJ perovskite solar cells.

Conclusions

We successfully incorporated fluorinated-PC_{61}BM to fabricate high performance and stable BHJ perovskite solar cells by single solvent and one-step solution process. The fluoroalkyl chain length of fluorinated-PC_{61}BM derivatives affects their self-aggregation behavior in the BHJ perovskite film. We show that 0.1 wt% of 3F-PC_{61}BM can be homogeneously dispersed in BHJ perovskite film and induce densely packed perovskite grains. Thus, a flat BHJ perovskite film is formed. The performance of device: J_{sc} and PCE can be increased from 19.96 mA/cm^2 and 14.12% of pristine device to 21.78 mA/cm^2 and 16.17 % of 0.1 wt% 3F-PC_{61}BM: perovskite BHJ device, respectively. On the other hand, the self-aggregation of 5F-PC_{61}BM molecules is easily formed in the BHJ perovskite film than that of 3F-PC_{61}BM molecules. That results in large amount of heterogeneous nucleation sites in the BHJ perovskite film for the formation of aggregated perovskite grains excessively with non-continuously rough film morphology. The voids in films would cause the directly contact between electron transporting layer and hole transporting layer, leading to poor device performance. Thus, the addition of 5F-PC_{61}BM decreases the PCE to be lower than that of the pristine device regardless its amount. We also show that the dense and flat surface morphology of 0.1 wt% 3F-PC_{61}BM: perovskite BHJ film can effectively suppress the permeation of moisture in ambient. The BHJ device can maintain 80% of their initial PCE over 550 hours while the pristine device degrades to lower than 80% after 240 hours storage. Our work provides a useful knowledge that by selecting proper fluoroalkyl chain and concentration of fluorinated-PC_{61}BM, we can easily fabricate high performance and high stability BHJ devices via a single solvent and simple one-step solution process.

Acknowledgements

The authors highly appreciated the financial support obtained from the Ministry of Science and Technology of Taiwan in this research (MOST 105-3113-E-002-010 and MOST 106-3113-E-002-008-CC2).

References

1 H. J. Snaith and M. Grätzel, *Adv. Mater.*, 2007, **19**, 3643-3647.
2 S. D. Stranks, G. E. Eperon, G. Grancini, C. Menelaou, M. J. P. Alcocer, T. Leijtens, L. M. Herz, A. Petrozza and H. J. Snaith, *Science*, 2013, **342**, 341-344.
3 L. M. Pazos-Outón, M. Szumilo, R. Lamboll, J. M. Richter, M. Crespo-Quesada, M. Abdi-Jalebi, H. J. Beeson, M. Vrućinić, M. Alsari, H. J. Snaith, B. Ehrler, R. H. Friend and F. Deschler, *Science*, 2016, **351**, 1430-1433.
4 Q. Dong, Y. Fang, Y. Shao, P. Mulligan, J. Qiu, L. Cao and J. Huang, *Science*, 2015, **347**, 967-970.
5 G. Xing, N. Mathews, S. Sun, S. S. Lim, Y. M. Lam, M. Grätzel, S. Mhaisalkar and T. C. Sum, *Science*, 2013, **342**, 344-347.
6 D. Shi, V. Adinolfi, R. Comin, M. Yuan, E. Alarousu, A. Buin, Y. Chen, S. Hoogland, A. Rothenberger, K. Katsiev, Y. Losovyj, X. Zhang, P. A. Dowben, O. F. Mohammed, E. H. Sargent and O. M. Bakr, *Science*, 2015, **347**, 519-522.
7 G. E. Eperon, S. D. Stranks, C. Menelaou, M. B. Johnston, L. M. Herz and H. J. Snaith, *Energy Environ. Sci.*, 2014, **7**, 982-988.
8 J. H. Noh, S. H. Im, J. H. Heo, T. N. Mandal and S. I. Seok, *Nano Lett.*, 2013, **13**, 1764-1769.

View Article Online
DOI: 10.1039/C7TA07939G

9 S. De Wolf, J. Holovsky, S. J. Moon, P. Loper, B. Niesen, M. Ledinsky, F. J. Haug, J. H. Yum and C. Ballif, *J. Phys. Chem. Lett.*, 2014, **5**, 1035-1039.
10 Q. Lin, A. Armin, R. C. R. Nagiri, P. L. Burn and P. Meredith, *Nature Photon.*, 2014, **9**, 106-112.
11 NREL, http://www.nrel.gov/ncpv/, updated 04/14/2017
12 A. Kojima, K. Teshima, Y. Shirai and T. Miyasaka, *Journal of the American Chemical Society*, 2009, **131**, 6050-6051.
13 W. S. Yang, J. H. Noh, N. J. Jeon, Y. C. Kim, S. Ryu, J. Seo and S. I. Seok, *Science*, 2015, **348**, 1234-1237.
14 H. S. Kim, C. R. Lee, J. H. Im, K. B. Lee, T. Moehl, A. Marchioro, S. J. Moon, R. Humphry-Baker, J. H. Yum, J. E. Moser, M. Gratzel and N. G. Park, *Sci. Rep.*, 2012, **2**, 591-597.
15 M. M. Lee, J. Teuscher, T. Miyasaka, T. N. Murakami and H. J. Snaith, *Science*, 2012, **338**, 643-647.
16 J. M. Ball, M. M. Lee, A. Hey and H. J. Snaith, *Energy Environ. Sci.*, 2013, **6**, 1739-1743.
17 T. Leijtens, G. E. Eperon, S. Pathak, A. Abate, M. M. Lee and H. J. Snaith, *Nat. Commun.*, 2013, **4**, 2885-2892.
18 Q. Chen, H. Zhou, Z. Hong, S. Luo, H. S. Duan, H. H. Wang, Y. Liu, G. Li and Y. Yang, *J. Am. Chem. Soc.*, 2014, **136**, 622-625.
19 K. Wojciechowski, M. Saliba, T. Leijtens, A. Abate and H. J. Snaith, *Energy Environ. Sci.*, 2014, **7**, 1142-1147.
20 H. Zhou, Q. Chen, G. Li, S. Luo, T. B. Song, H. S. Duan, Z. Hong, J. You, Y. Liu and Y. Yang, *Science*, 2014, **345**, 542-546.
21 J. Y. Jeng, Y. F. Chiang, M. H. Lee, S. R. Peng, T. F. Guo, P. Chen and T. C. Wen, *Adv. Mater.*, 2013, **25**, 3727-3732.
22 C. Y. Chang, C. Y. Chu, Y. C. Huang, C. W. Huang, S. Y. Chang, C. A. Chen, C. Y. Chao and W. F. Su, *ACS Appl. Mater. Interfaces*, 2015, **7**, 4955-4961.
23 J. Xu, A. Buin, A. H. Ip, W. Li, O. Voznyy, R. Comin, M. Yuan, S. Jeon, Z. Ning, J. J. McDowell, P. Kanjanaboos, J. P. Sun, X. Lan, L. N. Quan, D. H. Kim, I. G. Hill, P. Maksymovych and E. H. Sargent, *Nat. Commun.*, 2015, **6**, 7081-7088.
24 C. H. Chiang and C. G. Wu, *Nature Photon.*, 2016, **10**, 196-200.
25 M. Li, Y. H. Chao, T. Kang, Z. K. Wang, Y. G. Yang, S. L. Feng, Y. Hu, X. Y. Gao, L. S. Liao and C. S. Hsu, *J. Mater. Chem. A*, 2016, **4**, 15088-15094.
26 X. Liu, F. Lin, C. C. Chueh, Q. Chen, T. Zhao, P. W. Liang, Z. Zhu, Y. Sun and A. K. Y. Jen, *Nano Energy*, 2016, **30**, 417-425.
27 K. Wang, C. Liu, P. Du, J. Zheng and X. Gong, *Energy Environ. Sci.*, 2015, **8**, 1245-1255.
28 C. Liu, K. Wang, P. Du, C. Yi, T. Meng and X. Gong, *Adv. Energy Mater.*, 2015, **5**, 1402024-1402030.
29 M. Xiao, F. Huang, W. Huang, Y. Dkhissi, Y. Zhu, J. Etheridge, A. Gray-Weale, U. Bach, Y. B. Cheng and L. Spiccia, *Angew Chem. Int. Ed. Engl.*, 2014, **53**, 9898-9903.
30 N. Cho, H. L. Yip, S. K. Hau, K. S. Chen, T. W. Kim, J. A. Davies, D. F. Zeigler and A. K. Y. Jen, *J. Mater. Chem.*, 2011, **21**, 6956-6961.
31 W. Zhang, M. Saliba, D. T. Moore, S. K. Pathak, M. T. Horantner, T. Stergiopoulos, S. D. Stranks, G. E. Eperon, J. A. Alexander-Webber, A. Abate, A. Sadhanala, S. Yao, Y. Chen, R. H. Friend, L. A. Estroff, U. Wiesner and H. J. Snaith, *Nat. Commun.*, 2015, **6**, 6142-6151.
32 P. W. Liang, C. Y. Liao, C. C. Chueh, F. Zuo, S. T. Williams, X. K. Xin, J. Lin and A. K. Jen, *Adv. Mater.*, 2014, **26**, 3748-3754.
33 Y. C. Huang, C. S. Tsao, Y. J. Cho, K. C. Chen, K. M. Chiang, S. Y. Hsiao, C. W. Chen, C. J. Su, U. S. Jeng and H. W. Lin, *Sci. Rep.*, 2015, **5**, 13657-13667.

View Article Online
DOI: 10.1039/C7TA07939G

Table of Contents

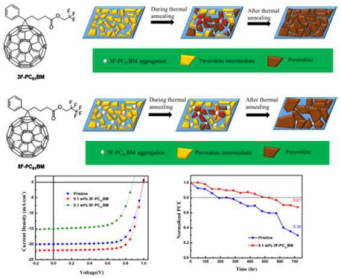

The fluorinated-$PC_{61}BM$ can be used to fabricate BHJ perovskite films by one-step using one solvent of BHJ precursor solution system.